ORIGINAL PAPER

Spatial coherence patterns of extreme winter precipitation in the U.S.

Abhirup Banerjee[1,2] · Matthias Kemter[1,2,3] · Bedartha Goswami[4] · Bruno Merz[2,3] · Jürgen Kurths[1,5] · Norbert Marwan[1,6]

Abstract

Extreme precipitation events have a significant impact on life and property. The U.S. experiences huge economic losses due to severe floods caused by extreme precipitation. With the complex terrain of the region, it becomes increasingly important to understand the spatial variability of extreme precipitation to conduct a proper risk assessment of natural hazards such as floods. In this work, we use a complex network-based approach to identify distinct regions exhibiting spatially coherent precipitation patterns due to various underlying climate mechanisms. To quantify interactions between event series of different locations, we use a nonlinear similarity measure, called the edit-distance method, which considers not only the occurrence of the extreme events but also their intensity, while measuring similarity between two event series. Using network measures, namely, degree and betweenness centrality, we are able to identify the specific regions affected by the landfall of atmospheric rivers in addition to those where the extreme precipitation due to storm track activity is modulated by different mountain ranges such as the Rockies and the Appalachians. Our approach provides a comprehensive picture of the spatial patterns of extreme winter precipitation in the U.S. due to various climate processes despite its vast, complex topography.

1 Introduction

Extreme precipitation poses a serious threat to lives and livelihood of people all around the world. With the intensification of extreme precipitation and increase in flood events over most climate regions (Tabari 2020; Easterling et al. 2017; Janssen et al. 2014; Vu and Mishra 2019; Kunkel et al. 2012) due to climate change, understanding the spatial variability of extreme precipitation is crucial

✉ Abhirup Banerjee
    abhirup.banerjee@pik-potsdam.de

1   Potsdam Institute for Climate Impact Research,
    Potsdam, Germany

2   Institute of Environmental Science and Geography,
    University of Potsdam, 14476 Potsdam, Germany

3   Helmholtz Centre Potsdam, GFZ German Research Centre
    for Geosciences, Potsdam, Germany

4   Cluster of Excellence Machine Learning: New Perspectives
    for Science, Universität Tübingen, Tübingen, Germany

5   Institute of Physics, Humboldt Universität zu,
    Berlin, Germany

6   Institute of Geoscience, University of Potsdam,
    14476 Potsdam, Germany

to manage the big socioeconomic losses often associated with them (Merz et al. 2021). Previous studies have shown that extreme precipitation connectivity in the United States (U.S.) is highest during the winter months (Touma et al. 2018), while river flood connectivity is higher in spring in the Rocky mountains and the central U.S. due to snow meltdown (Brunner et al. 2020). As reported in the billion-dollar weather and climate disasters catalog released by the NOAA/National Centers for Environmental Information (NCEI), in the period 2010–2020, 328 people were killed due to flooding and winter storms in the U.S. and more than $77 billion (U.S. dollars) worth of economic damages were caused (Weather 2021).

This included, for instance, the above-average precipitation leading to severe flooding in the Mississippi and Missouri Rivers and their tributaries during the winter season of 2019 (December 2018–February 2019) (Hoell et al. 2021; Flanagan et al. 2020). Therefore, our study focuses on extreme precipitation in the winter months (December–January–February; DJF), during which extreme rainfall may cause floods directly, and snowfall leads to the accumulation of snow packs for the melting season.

Numerous studies have analyzed extreme precipitation events across the U.S. (Mondal et al. 2020; Najibi et al. 2020) in terms of the meteorological causes of the

secular variations (Kunkel et al. 2012), their spatiotemporal variability (Mullen 2008), and their relation to large-scale meteorological patterns (Agel et al. 2019). Here, we focus on the spatial connectivity of extreme precipitation events, which is relevant for understanding river flood generation and anticipating the spatial extent of simultaneous flooding (Brunner et al. 2020; Kemter et al. 2020). Understanding the spatial dependence of extreme precipitation and its underlying mechanism is vital to assess risk from natural hazards. Simultaneous extreme precipitation across large scales can lead to synchronous flooding in multiple states, which has a greater societal and financial impact than independent, localized flood events due to regional interdependencies in risk management, infrastructure, and insurance (Jongman et al. 2014).

We use a complex network-based approach to study the spatial patterns of extreme winter precipitation in the U.S. Climate network analysis can help to identify the regions which are most likely to experience concurrent precipitation extremes along with the climatic conditions that are responsible for their generation. The climate network belongs to the category of *functional network*, in which pairwise statistical dependencies between the time series associated with the nodes of the network are computed to estimate the functional connectivity between them. Then, the topological structure of the network is analyzed using different network measures (Donges et al. 2009b; Fan et al. 2021; Tsonis and Roebber 2004).

The network representation of the spatiotemporal climate data allows us to study pairwise interactions between climate variables of different locations. The analysis of the climate network enables us to understand the spatial pattern of climate variability. Standard similarity measures used to estimate the strength of the climate interaction include Pearson's or Spearman's correlation coefficients. However, these are not suitable for evaluating the relationship within extreme precipitation data, which are event-like time series. Therefore, nonlinear synchronization measures specifically designed to compute the similarity between event series are required to construct extreme precipitation networks. Recent works have extensively used *event synchronization* (ES) (Quian Quiroga et al. 2002), in particular, to construct climate networks for event-like data such as extreme precipitation (Malik et al. 2011; Stolbova et al. 2014; Ozturk et al. 2019) and heat wave pattern (Mondal and Mishra 2021). Boers et al. (2013), Boers et al. (2014a), and Boers et al. (2014b) used complex networks constructed based on ES to study the South American Monsoon and reveal the global extreme precipitation pattern (Boers et al. 2019). Konapala and Mishra (2017) used the same climate network framework to study hydroclimatic extreme events. Agarwal et al. (2017) introduced multi-scale event synchronization by combining wavelet transform and ES. However, ES only

considers the time of occurrence of events to identify the events' coincidence and obtain the degree of similarity, but not the difference in strength or amplitude of the events. While some previous works (Ciemer et al. 2018) have proposed some modified correlation measures to investigate spatial co-variability patterns of general precipitation (i.e., considering the amplitude variability), they are linear and, thus, limited for studying extreme precipitation behavior.

In our study, we use a special distance metric, particularly designed to study the similarity between spike trains, called *edit distance* (ED), first proposed by Victor and Purpura (1997) and later extended by Hirata and Aihara (2009). This metric has been used in combination with recurrence plots (Eckmann 1987) to analyze the recurrence property of marked point process data (Suzuki et al. 2010), paleoclimate data (Ozken et al. 2015; Ozken et al. 2018), and extreme event-like hydrological data (Banerjee et al. 2021). Recently, Agarwal et al. (2022) integrated ED with climate networks to study the extreme rainfall pattern in the Ganga River basin and highlighted its advantage over ES. In the case of ED, each event series is considered as a marked point process and the similarity between two such event series is measured by optimizing the cost of transformation associated with transforming one event series to another one through elementary operations, such as shifting in time or amplitude, addition, or deletion of events.

Spatial patterns of different network measures, namely the degree and the betweenness centrality, are used to study the spatial connectivity pattern of extreme winter (DJF) precipitation events. While the degree centrality is based on local topological information, the path-based betweenness centrality includes the global topological information (Donges et al. 2009b). Through our approach, we are not only able to identify regions with distinct extreme precipitation patterns, but also delineate the regions affected by atmospheric rivers and tornadoes. In Section 2, we describe in detail the data and the methodology. In Section 3, we discuss the results based on our network analysis and draw an interpretation from a climatological point of view.

2 Data and methodology

2.1 Data source and data pre-processing

In this study, we use daily averaged precipitation, geopotential height and wind at different pressure levels, and vertically integrated water vapor (IVT) flux data derived from ERA5 reanalysis (Hersbach et al. 2020) for the period 1980–2020. The spatial resolution used is $0.5° \times 0.5°$. It is worth mentioning here that although the reanalysis precipitation data do show biases compared to the

observations, observational datasets typically either have a limited spatial coverage (GPCC, TRMM, etc.), lower resolution (GPCP), or a limited temporal coverage (TRMM). The ERA5 shows, in most cases, smaller biases than other reanalysis datasets (JRA-55, MERAA-2) (Hassler and Lauer 2021). Nevertheless, we verify the robustness of our results by comparing them with those obtained using JRA-55 (Japan Meteorological Agency 2013) (see figures in the Supporting information).

To construct the extreme precipitation event series from the daily averaged precipitation time series data at each grid point, we consider only those days as events for which precipitation is among the highest 5% of all values, including dry days without precipitation, in a particular season (here, DJF) at that location, resulting in 4 to 5 events for each season (Malik et al. 2011; Boers et al. 2013; Stolbova et al. 2014).

2.2 Network construction

A network or graph comprises two main components: a set of nodes V and a collection of edges E. Mathematically, a network is expressed as $G = \{V, E\}$ (Donges et al. 2009b; Sivakumar and Woldemeskel 2014). In the case of a climate network, each geographical grid point of the climate dataset is considered a node, and an edge is placed when there is a statistically significant association or functional dependency between two nodes. To construct the climate network for extreme precipitation, first, we transform the precipitation time series data at each grid point into an extreme precipitation event series as described earlier.
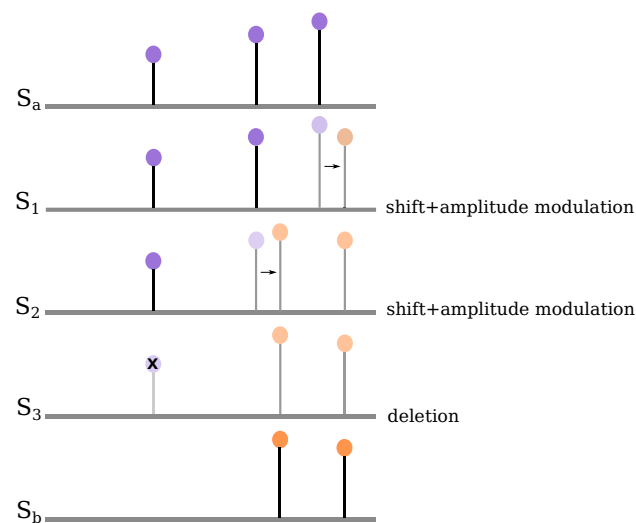

Fig. 1 Schematic of the transformation of segment S_a to S_b through four steps numbered as steps $S_1, \ldots, S_3$. The path shown is a minimal-cost path and all steps are elementary steps, i.e., shifting an event, amplitude modulation, deleting/inserting

Then, we construct the network for extreme precipitation events to study its pattern of spatial variability as follows.

In this study, we use the edit distance (ED) method, which takes into account both the sequence and amplitude of events. In general, ED is a distance metric to quantify the similarity/ dissimilarity between two spike trains (Victor and Purpura 1997; Banerjee et al. 2021). Additionally, ED considers each event series as a marked point process (Suzuki et al. 2010; Ozken et al. 2015; Ozken et al. 2018). The idea is to transform an event series into another series by performing some elementary operations: shifting in time, amplitude modulation, and deletion/insertion of events (Fig. 1). A specific cost is assigned to each such operation. The total transformation cost to convert one event series to the other is computed by tracing the minimal-cost path.

The mathematical formulation of the distance metric is described as follows. Consider two given segments S_a and S_b, the minimum cost of transformation is defined as

$$D(S_a, S_b) = \min_{C} \left\{ \left\{ \sum_{(\alpha,\beta) \in C} \Lambda_0 \|t_a(\alpha) - t_b(\beta)\| + \Lambda_1 \|L_a(\alpha) - L_b(\beta)\| \right\} + \Lambda_s (|I| + |J| - 2|C|) \right\}. \quad (1)$$

The time and amplitude of events are denoted as $t_a(\alpha)$, $t_b(\beta)$, and $L_a(\alpha)$, $L_b(\beta)$, Λ_0 and Λ_1 are the coefficient of cost of shifting in time and change in amplitude, while the cost allotted for each insertion and deletion operation is Λ_s. The first term of Eq. (1) sums the cost of shifting in time and amplitude modulation between the αth event in S_a and βth event in S_b. C is the set containing all the pairs associated in this operation. The second term in Eq. (1) denotes the deletion/insertion operation. I, J are the sets of indices of events in S_a and S_b respectively. $|I|$, $|J|$, and $|C|$ are the cardinalities of the sets I, J, and C respectively. All three cost parameters are computed as suggested by Agarwal et al. (2022).

Naturally, the minimum cost of transformation implies the highest similarity and vice versa. We then calculate the transformation cost for every pair of event series S_i and S_j, corresponding to nodes i and j, of the gridded extreme event dataset using the above method, which gives us the similarity matrix Q_{ij} (here, cost matrix). Thereafter, we obtain the adjacency matrix A_{ij} by thresholding the similarity matrix Q_{ij} with a suitable threshold, which gives the edges of our network. Mathematically, $A_{ij} = \Theta(\epsilon - Q_{ij}) - \delta_{ij}$, where Θ is the Heaviside function, i.e., we assign 1 when the cost is below a certain threshold, otherwise 0. ϵ is the threshold, and δ_{ij} is the Kronecker delta to remove self loops. In the case of ED, lower transformation cost

between two event series implies higher similarity. For all pairs of grid cells whose value of the transformation cost is below the threshold ϵ will be connected by an edge. In this study, to find the significant edges, we fix the edge density of the network at $\rho = \frac{2E}{N(N-1)} = 5\%$ and choose the corresponding threshold $\epsilon(\rho)$ (Malik et al. 2011; Stolbova et al. 2014; Wiedermann et al. 2017).

2.3 Network measures

Various network measures are used to quantify the network topology which provide novel insights into the underlying dynamics of the system over different spatial scales (Donges et al. 2009a). We use two network measures to quantify and characterize the spatial pattern of extreme precipitation. One of the basic local network measures is the *degree* which measures the centrality of a node based on how well-connected it is. The degree k_i of a node i is defined as

$$k_i = \sum_{j=1}^{N} A_{ij} \tag{2}$$

where N is the total number of grid points (nodes). It quantifies the number of direct connections node i has with other nodes in the network (Fig. 2a).

In climate networks, nodes connected by a link indicate the spatial distribution of areas with similar climate variability. The nodes with higher degree values k_i are crucial regions that regulate the connectivity of the network and are typically related to large-scale atmospheric circulation (Malik et al. 2011; Boers et al. 2013; Boers et al. 2014b). Degree has been used to identify the highly connected geographical sites (super-nodes) and their association with atmospheric teleconnection pattern (Tsonis et al. 2008; Radebach et al. 2013; Agarwal et al. 2019).

The second network measure we use here is the *betweenness centrality*, which provides information about the global topology of the network on the basis of shortest paths between pairs of nodes (Donges et al. 2009a).

Betweenness centrality BC_i measures how much a node i falls "in between" two nodes in the network, i.e., acts as a bridge connecting two other nodes (Newman 2010; Freeman 1978). A node may not be well-connected (i.e., has low degree) but can be crucial to connect different parts of the network (Golbeck 2015) (Fig. 2b). Betweenness is quantified by measuring the percentage of the shortest paths that must go through this specific node i and is defined as

$$BC_i = \sum_{j,k \neq i}^{N} \frac{\sigma_{jk}(i)}{\sigma_{jk}} \tag{3}$$

where σ_{jk} is the total number of shortest path between node j and k and $\sigma_{jk}(i)$ is the number of shortest paths that go via node i. In the case of a social network, BC indicates the importance of a node in controlling the flow of information in the network. However, for functional networks, such as climate networks, it represents boundaries between highly connected regions (Molkenthin et al. 2014; Tupikina et al. 2016). BC has been used to uncover energy flow patterns in the atmosphere (Donges et al. 2009b) and has also been successfully applied to study the extreme precipitation patterns of different monsoon systems (Boers et al. 2013; Stolbova et al. 2014).

Correction for spatial embedding: When we choose a particular study area, we impose an artificial boundary in space. These boundaries influence the climate network (Rheinwalt et al. 2012; Boers et al. 2013) by cutting links that actually connect nodes with outer regions, hence affecting the network measures. Here we adopt the boundary correction procedure suggested by Rheinwalt et al. (2012) as follows: We first generate 500 spatially embedded random networks (Barnett et al. 2007) (SERN) which preserve both the node position and the distribution of the spatial link lengths of the original network. After that, we compute the network measures for all SERN surrogates. The boundary-corrected network measure is obtained by dividing the value of the measure of the original network by that of the average of the SERN surrogates.
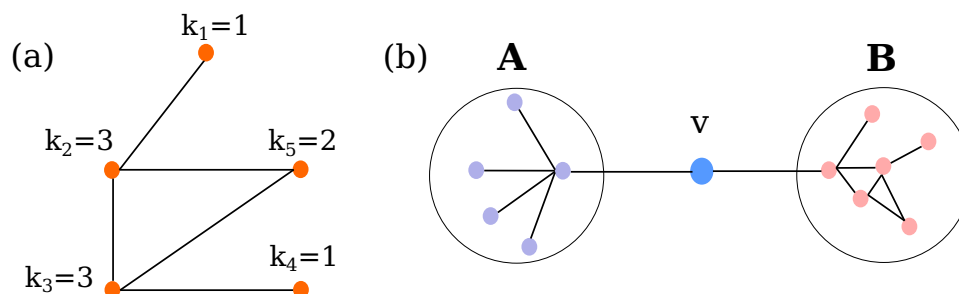

Fig. 2 Network measures: (a) Degree k_i of the network nodes, based on the number of connections of node i with other nodes. Degree measures how well-connected a node is in the network. (b) Betweenness centrality BC_i of network nodes. Node v has low degree but high betweenness because it acts as a bridge joining two groups of nodes A and B
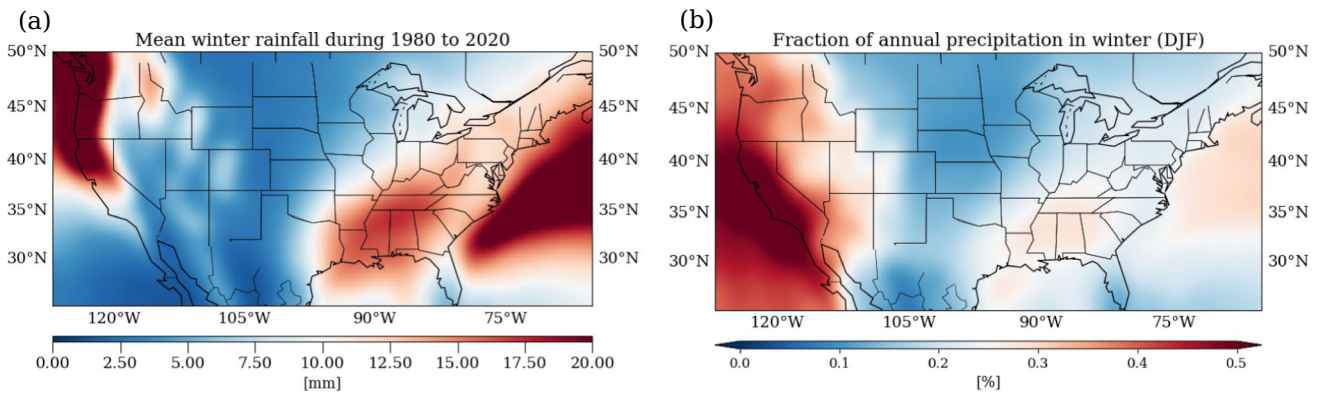
(a)

(b)

Fig. 3 (a) Mean daily winter precipitation from 1980 to 2020. (b) Mean winter precipitation anomaly as the fraction of mean annual precipitation falling in winter (same period) for ERA5 reanalysis data.

Anomalies are highly positive along the West Coast and slightly positive along the southern flank of the Appalachians. Highly negative anomalies exist in the central north

3 Results and discussion

3.1 Calculation and network interpretation

In this section, we analyze the winter extreme precipitation pattern of the U.S. using the above introduced complex network measures. Our climate network, constructed using the ED metric (mentioned in Section 2.2), considers both the sequence and the amplitude of events when quantifying similarity. High degree nodes (Eq. 2) represent regions of high connectivity of extreme precipitation events that are connected to many grid cells which exhibit similar variability of extreme precipitation occurrence and intensity. We find in our extreme precipitation network, a relatively low degree in the northwestern part of the U.S. (Fig. 4a), suggesting less similarity of extreme precipitation behavior with any other regions. On the other hand, a high degree is observed in the eastern Pacific Ocean and southwestern part of the U.S. To understand the connectivity pattern for these regions, we choose really small boxes **A** (low degree) and **B** (high degree), in the northwestern part of the U.S. and in the eastern Pacific Ocean respectively, and determine the

number of links connecting these boxes with other nodes in the network (Fig. 5a and b). We find that connections with the region **A** are confined to a very small region centered more towards the coast, indicating a quite narrow corridor of moisture transport as typical for atmospheric rivers (Dettinger 2013; Xiong and Ren 2021; Hu et al. 2017; Gonzales et al. 2019). On the other hand, the connectivity of region **B** spans over a larger area in the Pacific Ocean and extending up to some parts of the southwestern coast. Such extended spatial connectivity of extreme precipitation indicates the presence of a larger atmospheric pattern that impacts the region, such as tropical cyclones which usually tend to cause enhanced rainfall in this region (Woodruff et al. 2013).

We also observe high degree values in the Great Plains and northeastern parts of the U.S. We choose another small box **C** in this region which lies roughly in the Mississippi river watershed (Fig. 5c). The connectivity pattern of this region indicates similar variability of extreme precipitation along the southwest-northeast direction. Furthermore, high-elevation regions such as the Cascades, some parts of the Rockies and the Appalachians show relatively lower degree
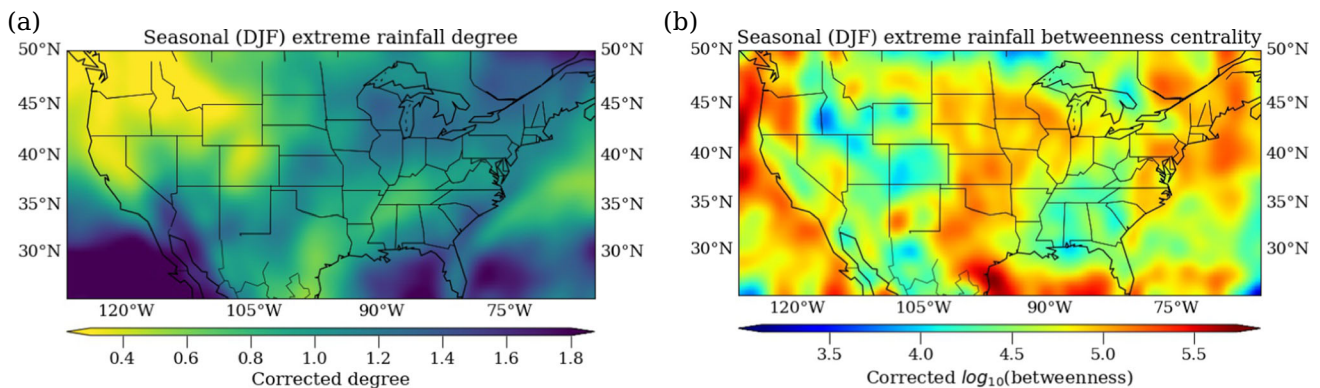
(a)

(b)

Fig. 4 (a) Degree and (b) betweenness centrality for extreme winter (DJF) precipitation from 1980 to 2020
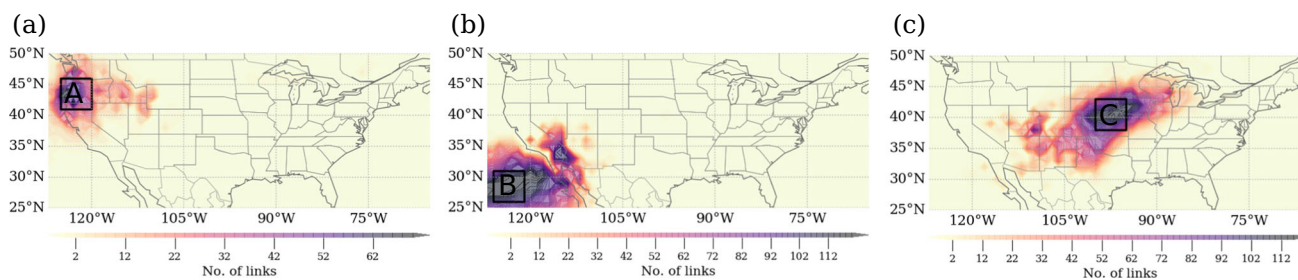
Fig. 5 Partial degree, i.e., the number links connected to the selected regions in the north-western U.S. (box A), eastern Pacific Ocean (box B), and in the central U.S. (box C)

than regions of low elevation which was also observed by Agarwal et al. (2022) in case of extreme precipitation networks constructed using edit-distance for the Ganges river basin in India. Similar observations are made in the results obtained using JRA-55 dataset (see Fig. S2a).

Next, we study the spatial patterns of *BC* (Fig. 4b), which reveal some striking structures associated with the transition zones between different atmospheric flows (Molkenthin et al. 2014; Tupikina et al. 2016) during winter in the U.S.

Along the northwestern coast of the U.S., we find high betweenness but low degree. This implies that although these are relatively small regions of similar precipitation dynamics, they are transition zones of different atmospheric flow directions (Molkenthin et al. 2014), possibly because of spatial confinement and orographic lift due to the presence of topographical features such as mountains. The high *BC* values are seen to continue downwards along the entire western coast, lining the land-sea boundary. The results obtained from ERA5, however, deviate from those obtained from JRA-55, where the *BC* values decrease substantially beyond 30°N southwards.

We observe high BC values in the central U.S., i.e., from Texas towards the Midwest area, and in the northeastern region, which are also regions of high degree. This implies that while the lower elevation regions, east of the Rocky mountains (Great Plains) and the Appalachians (Coastal Plains), are large regions of spatially coherent extreme precipitation dynamics, big rivers, and mountain features cause diversification of atmospheric flow leading to different and strongly fragmented precipitation patterns. These observations are mostly similar with those seen in the network constructed using the JRA-55 dataset (Fig. S2b) except for the small disparity in BC values seen along the southwest coast. This may be due to the relatively high bias in JRA-55 precipitation data in the Pacific Ocean close to the tropics (Hassler and Lauer 2021).

3.2 Climatological interpretation

The low spatial connectivity of precipitation in the northwestern part of the U.S. (Fig. 4a) is caused due to the effects of the Cascade and Rocky Mountains. Precipitation gets "trapped" west of these ranges and, thus, is not connected to the rest of the country, lowering the overall degree. At higher elevations, extreme precipitation requires different conditions than the coast, so the northwest coast and the mountain ranges are also not connected. However, as rainstorms can travel more freely through the plains on the eastern side of the mountains, it leads to a higher regional similarity. The presence of the western Cascades results into an orographic lift, effectively transforming the water vapor to extreme precipitation resulting in high BC values a little inland from the northwest coast (Fig. 4b).

The southwestern part of the U.S. along with adjacent regions of the eastern Pacific Ocean exhibits high connectivity due to a high fraction of winter precipitation despite low mean winter precipitation (Fig. 3). This can be explained by the fact that this part of the eastern Pacific is a separate, relatively small, and well-organized precipitation system (Zhang and Wang 2021) as also seen from Fig. 5b. Elevation and slopes are much lower here than further north, so rainstorms can penetrate further into the land and cause near-simultaneous precipitation along the land terrain.

The southwestern coast has high BC values similar to the northwestern coast, indicating that they may be related to the transition in opposing atmospheric flow direction. The western coast of the U.S. experiences heavy precipitation, and hence extreme streamflows, due to the atmospheric rivers (ARs), which contribute 30 to 45% of total winter precipitation (Dettinger 2013; Xiong and Ren 2021; Hu et al. 2017). ARs are relatively narrow filament-shaped conduits of moisture in the atmosphere transported from the lower latitudes to the mid and high latitudes (Gimeno et al. 2016; Guan and Waliser 2015;

Ralph et al. 2019). The activity of ARs starts during autumn and tends to shift southward along the Pacific coast later during the winter (Gonzales et al. 2019). However, these ARs may be associated with different regimes of large-scale Rossby wave breaking (RWB) — anticyclonic wave breaking (AWB) in the northwest and cyclonic wave breaking (CWB) in the southwest (Hu et al. 2017)(Fig. 6a and b). The penetration of high BC values further inland (Fig. 4b), in the northwest U.S., close to the western slope of the Cascades may be related to the AWB-ARs, which arrive more orthogonally to the western Cascades due to their westerly impinging angle transforming moisture to precipitation due to orographic lift. On the other hand, the CWB-ARs have impinging angles, which are more southwesterly, and therefore arrive more orthogonally to the east-west oriented Olympics in the northwest U.S. and the northwest-southeast oriented Sierra Nevada along the southwest coast. Consequently, they cause intense precipitation along the western coast. The transformation of water vapor to extreme precipitation through the orographic lift (Barlow et al. 2019), albeit due to different regimes of RWB, explains the high BC along the western coast. The relatively high degree in the southwestern region may be related to the high density of the shorter track ARs close to central and southern California. The seasonal progression

of the mean latitude position of the AR tracks southwards could also possibly explain the high BC values in this region (Gonzales et al. 2019).

The southwest-northeast (SW-NE) inclination in connectivity of the high degree regions in the northeast U.S. and the Great Plains (Fig. 5c) is in agreement with (Najibi et al. 2020), who found high similarity in anomalous extreme precipitation in winter in these regions.

The eastern side of the Rockies also has high BC values, which may be attributed to the pressure gradient seen in the atmosphere (Fig. 6a, b, and c) (Molkenthin et al. 2014). The area roughly coincides with the loosely defined region called the Tornado Alley, where tornadoes occur very frequently (Concannon and Brooks 2000; Bluestein 2006). We also see the propagation of wind in the southwesterly direction in all atmospheric levels (Fig. 6a, b, and c). The IVT seasonal composite anomalies (Fig. 6d) also show an anomalously high moisture transport in this direction. This flow pattern is modulated by the presence of the Rocky mountains (Lukens et al. 2018) which suppress the storm-track activity by deflecting the westerly flow over land (Chang 2009). This leads to a SW-NE tilt in the upper tropospheric jet (Fig. 6a) which subsequently causes a downstream flow and hence high betweenness along those nodes.
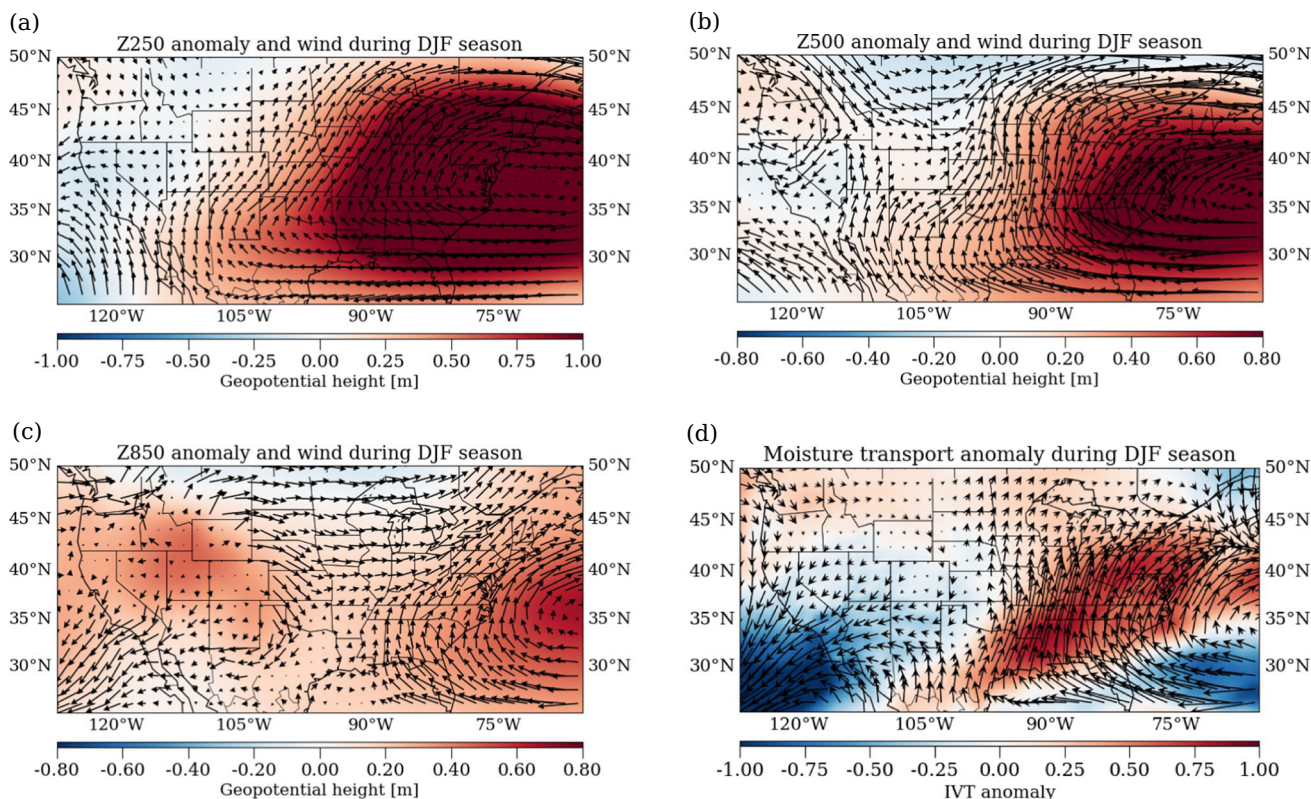

Fig. 6 (a–c) Geopotential height and wind in 250hPa, 500hPa, and 850hPa atmospheric level. (d) Vertically integrated water vapor flux anomaly during winter season (DJF)

High *BC* values along the northeast coast of the U.S. may also be associated with high baroclinic instability formed due to the large land-sea temperature gradient in winter over northeastern U.S. Brayshaw et al. (2009) which leads to an intensification of extratropical storms on the leeward side of the Appalachian mountains (Colucci 1976; Lukens et al. 2018). Extreme precipitation in this region is mainly related to an anomalously high upward lift of air along the coast due to high vorticity advection, frequent warm conveyor belts, and diabatic heating (Agel et al. 2019). The wind flow (Fig. 6a, b, and c) and high anomalous IVT (Fig. 6d), along the northeast coast, lead to synchronous extreme precipitation in the region and hence high degree.

4 Conclusions

The climate network approach has been proven to be a robust and promising framework for studying various climate extremes such as extreme monsoon precipitation (Malik et al. 2011; Boers et al. 2013; Boers et al. 2014b), the influence of El Niño (Boers et al. 2014a), and cyclone tracks (Gupta et al. 2021). In this work, we studied the spatial variability of extreme precipitation during winter in the U.S., which has a very complex topography. For this, we employ the edit distance metric to measure pairwise similarity between extreme precipitation time series of different locations. Most of the earlier developed methods (Malik et al. 2011; Stolbova et al. 2014; Boers et al. 2013; Boers et al. 2014a; Wolf et al. 2020) consider only the timing of events when studying the similarities in event-like data. However, the edit distance emerges as a powerful alternative measure because it considers the amplitude or strength of extreme events along with their time of occurrence when calculating the similarity.

Extension of the coherent regions depends on the orography, seasonal climatology, and the presence of any atmospheric circulation. Understanding the spatial extent of regions of coherent extreme precipitation is necessary for risk assessment of natural hazards. Through a combination of network measures, viz., degree and betweenness centrality, we were able to identify the different regions of the U.S. which exhibit distinctly different extreme precipitation dynamics. While the analysis of the spatial patterns of degree differentiated between extreme precipitation variability of the northwest and the southwest coast based on the associated large-scale atmospheric circulation, the high betweenness along the entire western coast brought to light the role of atmospheric rivers and that of topographic barriers in causing extreme precipitation. The network measures also demarcated the "Tornado Alley" (Concannon and Brooks 2000; Bluestein 2006) region in the Great Plains where tornadoes are more frequent. The high degree

pattern captured the southwest-northeast (SW-NE) inclination (Najibi et al. 2020; Lukens et al. 2018) of extreme precipitation due to modulation of storms by the Rocky mountains. Similarly, a modulation of extreme precipitation due to other high ranges, such as the western Cascades and the Appalachians in the east of the country, was also reflected in the network connectivity.

Our complex network-based approach provides a comprehensive overview of the distinct regions which experience spatially coherent extreme winter precipitation in the U.S. albeit due to various climate processes. The similarity measure used in this study, the edit distance, comes out as a very promising alternative to studying extreme precipitation patterns in regions exhibiting very intricate climate variability, such as the U.S. Future work may include studying the effects of increasing intensity of extreme precipitation for different large-scale monsoon systems and to possibly identify teleconnections.

Declarations

References

Agarwal A, Caesar L, Marwan N, Maheswaran R, Merz B, Kurths J (2019) Network-based identification and characterization of teleconnections on different scales. Scientific Reports 9

Agarwal A, Guntu RK, Banerjee A, Gadhawe MA, Marwan N (2022) A complex network approach to study the extreme precipitation patterns in a river basin. Chaos: An Interdisciplinary Journal of Nonlinear Science 32(1):013113

Agarwal A, Marwan N, Rathinasamy M, Merz B, Kurths J (2017) Multi-scale event synchronization analysis for unravelling climate processes: a wavelet-based approach. Nonlinear Process Geophys 24(4):599–611. https://doi.org/10.5194/npg-24-599-2017. https://npg.copernicus.org/articles/24/599/2017/

Agel L, Barlow M, Colby F, Binder H, Catto J, Hoell A, Cohen J (2019) Dynamical analysis of extreme precipitation in the us northeast based on large-scale meteorological patterns. Clim Dyn 52:1–22. https://doi.org/10.1007/s00382-018-4223-2

Banerjee A, Goswami B, Hirata Y, Eroglu D, Merz B, Kurths J, Marwan N (2021) Recurrence analysis of extreme event-like data. Nonlinear Process Geophys 28(2):213–229. https://npg.copernicus.org/articles/28/213/2021/

Barlow M, Gutowski W, Gyakum J, Katz R, Lim Y, Schumacher R, Wehner M, Agel L, Bosilovich M, Collow A, Gershunov A, Grotjahn R, Leung R, Milrad S, Min S (2019) North american extreme precipitation events and related large-scale meteorological patterns: a review of statistical methods, dynamics, modeling, and trends. Clim Dyn 53:6835–6875

Barnett L, Di Paolo E, Bullock S (2007) Spatially embedded random networks. Phys Rev E 76:056115. https://doi.org/10.1103/PhysRevE.76.056115

Bluestein HB (2006) Tornado alley: monster storms of the Great Plains. Oxford University Press, New York

Boers N, Bookhagen B, Marwan N, Kurths J, Marengo J (2013) Complex networks identify spatial patterns of extreme rainfall events of the South American Monsoon System. Geophys Res Lett 40(16):4386–4392. https://doi.org/10.1002/grl.50681

Boers N, Donner R, Bookhagen B, Kurths J (2014a) Complex network analysis helps to identify impacts of the el niño southern oscillation on moisture divergence in South America. Clim Dyn 45:1–14. https://doi.org/10.1007/s00382-014-2265-7

Boers N, Goswami B, Rheinwalt A, Bookhagen B, Hoskins B, Kurths J (2019) Complex networks reveal global pattern of extreme-rainfall teleconnections. Nature 566(7744):373–377. https://doi.org/10.1038/s41586-018-0872-x

Boers N, Rheinwalt A, Bookhagen B, Barbosa HMJ, Marwan N, Marengo J, Kurths J (2014b) The South American rainfall dipole: a complex network analysis of extreme events. Geophys Res Lett 41(20):7397–7405. https://doi.org/10.1002/2014GL061829

Brayshaw DJ, Hoskins B, Blackburn M (2009) The basic ingredients of the North Atlantic storm track. Part I: Land-sea contrast and orography. J Atmos Sci 66(9):2539–2558. https://doi.org/10.1175/2009JAS3078.1

Brunner MI, Gilleland E, Wood A, Swain DL, Clark M (2020) Spatial dependence of floods shaped by spatiotemporal variations in meteorological and land-surface processes. Geophys Res Lett 47(13):e2020GL088000. https://doi.org/10.1029/2020GL088000

Chang EKM (2009) Diabatic and orographic forcing of northern winter stationary waves and storm tracks. J Clim 22(3):670–688. https://doi.org/10.1175/2008JCLI2403.1. https://journals.ametsoc.org/view/journals/clim/22/3/2008jcli2403.1.xml

Ciemer C, Boers N, Barbosa H, Kurths J, Rammig A (2018) Temporal evolution of the spatial covariability of rainfall in south america. Climate Dynamics 51, https://doi.org/10.1007/s00382-017-3929-x

Colucci SJ (1976) Winter cyclone frequencies over the eastern United States and adjacent western Atlantic, 1964–1973: student paper–first place winner of the father James B. Macelwane annual award in meteorology, announced at the annual meeting of the AMS, Philadelphia, PA., 21 January 1976. Bull Am Meteor Soc 57(5):548–553. https://doi.org/10.1175/1520-0477(1976)057⟨0548:WCFOTE⟩2.0.CO;2

Concannon P, Brooks H (2000) Climatological risk of strong and violent tornadoes in the United States

Dettinger MD (2013) Atmospheric rivers as drought busters on the U.S. west coast. J Hydrometeorol 14(6):1721–1732. https://doi.org/10.1175/JHM-D-13-02.1. https://journals.ametsoc.org/view/journals/hydr/14/6/jhm-d-13-02_1.xml

Donges JF, Zou Y, Marwan N, Kurths J (2009) Complex networks in climate dynamics. The European Physical Journal Special Topics 174(1):157–179

Donges JF, Zou Y, Marwan N, Kurths J (2009) The backbone of the climate network. EPL Europhysics Letters 87(4):48007. https://doi.org/10.1209/0295-5075/87/48007

Easterling DR, Kunkel KE, Arnold JR, Knutson T, LeGrande AN, Leung LR, Vose RS, Waliser DE, Wehner MF (2017) Precipitation change in the United States, U.S. Global Change Research Program, Washington, D.C., pp. 207–230. https://doi.org/10.7930/J0H993CC

Eckmann J (1987) Kamphorst so, ruelle d. Recurrence plots of dynamical systems Europhys Lett 4:973–977

Fan J, Meng J, Ludescher J, Chen X, Ashkenazy Y, Kurths J, Havlin S, Schellnhuber HJ (2021) Statistical physics approaches to the complex earth system. Phys Rep 896:1–84. https://doi.org/10.1016/j.physrep.2020.09.005. https://www.sciencedirect.com/science/article/pii/S0370157320303458, statistical physics approaches to the complex Earth system

Flanagan PX, Mahmood R, Umphlett NA, Haacker E, Ray C, Sorensen W, Shulski M, Stiles CJ, Pearson D, Fajman P (2020) A hydrometeorological assessment of the historic 2019 flood of Nebraska, Iiowa, and South Dakota. Bull Am Meteor Soc 101(6):E817–E829. https://doi.org/10.1175/BAMS-D-19-0101.1

Freeman LC (1978) Centrality in social networks conceptual clarification. Social Networks 1(3):215–239. https://doi.org/10.1016/0378-8733(78)90021-7. https://www.sciencedirect.com/science/article/pii/0378873378900217

Gimeno L, Dominguez F, Nieto R, Trigo R, Drumond A, Reason CJ, Taschetto AS, Ramos AM, Kumar R, Marengo J (2016) Major mechanisms of atmospheric moisture transport and their role in extreme precipitation events. Annu Rev Environ Resour 41(1):117–141. https://doi.org/10.1146/annurev-environ-110615-085558

Golbeck J (2015) Chapter 21 - analyzing networks. In: Golbeck J (ed) Introduction to Social Media Investigation. Syngress, Boston, pp 221–235. https://doi.org/10.1016/B978-0-12-801656-5.00021-4, https://www.sciencedirect.com/science/article/pii/B9780128016565000214

Gonzales KR, Swain DL, Nardi KM, Barnes EA, Diffenbaugh NS (2019) Recent warming of landfalling atmospheric rivers along

the west coast of the United States. Journal of Geophysical Research: Atmospheres 124(13):6810–6826. https://doi.org/10.1029/2018JD029860

Guan B, Waliser DE (2015) Detection of atmospheric rivers: evaluation and application of an algorithm for global studies. Journal of Geophysical Research: Atmospheres 120(24):12514–12535. https://doi.org/10.1002/2015JD024257

Gupta S, Boers N, Pappenberger F, Kurths J (2021) Complex network approach for detecting tropical cyclones. Climate Dynamics. https://doi.org/10.1007/s00382-021-05871-0

Hassler B, Lauer A (2021) Comparison of reanalysis and observational precipitation datasets including ERA5 and WFDE5. Atmosphere 12(11):1462. https://doi.org/10.3390/atmos12111462. https://www.mdpi.com/2073-4433/12/11/1462

Hersbach H, Bell B, Berrisford P, Hirahara S, Horányi A, Muñoz-Sabater J, Nicolas J, Peubey C, Radu R, Schepers D, Simmons A, Soci C, Abdalla S, Abellan X, Balsamo G, Bechtold P, Biavati G, Bidlot J, Bonavita M, De Chiara G, Dahlgren P, Dee D, Diamantakis M, Dragani R, Flemming J, Forbes R, Fuentes M, Geer A, Haimberger L, Healy S, Hogan RJ, Hólm E, Janisková M, Keeley S, Laloyaux P, Lopez P, Lupu C, Radnoti G, de Rosnay P, Rozum I, Vamborg F, Villaume S, Thépaut JN (2020) The era5 global reanalysis. Q J R Meteorol Soc 146(730):1999–2049. https://doi.org/10.1002/qj.3803. https://rmets.onlinelibrary.wiley.com/doi/abs/10.1002/qj.3803

Hirata Y, Aihara K (2009) Representing spike trains using constant sampling intervals. J Neurosci Methods 183(2):277–286. https://doi.org/10.1016/j.jneumeth.2009.06.030. http://www.sciencedirect.com/science/article/pii/S0165027009003513

Hoell A, Hoerling M, Eischeid J, Barsugli J (2021) Preconditions for extreme wet winters over the contiguous United States. Weather and Climate Extremes 33:100333. https://doi.org/10.1016/j.wace.2021.100333. https://www.sciencedirect.com/science/article/pii/S2212094721000311

Hu H, Dominguez F, Wang Z, Lavers DA, Zhang G, Ralph FM (2017) Linking atmospheric river hydrological impacts on the U.S. West Coast to Rossby wave breaking. J Clim 30(9):3381–3399. https://doi.org/10.1175/JCLI-D-16-0386.1. https://journals.ametsoc.org/view/journals/clim/30/9/jcli-d-16-0386.1.xml

Janssen E, Wuebbles DJ, Kunkel KE, Olsen SC, Goodman A (2014) Observational- and model-based trends and projections of extreme precipitation over the contiguous United States. Earth's Future 2(2):99–113. https://doi.org/10.1002/2013EF000185

Japan Meteorological Agency, Japan (2013) Jra-55: Japanese 55-year reanalysis, daily 3-hourly and 6-hourly data. https://doi.org/10.5065/D6HH6H41

Jongman B, Hochrainer-Stigler S, Feyen L, Aerts JC, Mechler R, Botzen WW, Bouwer LM, Pflug G, Rojas R, Ward PJ (2014) Increasing stress on disaster-risk finance due to large floods. Nat Clim Chang 4(4):264–268

Kemter M, Merz B, Marwan N, Vorogushyn S, Blöschl G (2020) Joint trends in flood magnitudes and spatial extents across Europe. Geophys Res Lett 47(7):1–8. https://doi.org/10.1029/2020GL087464

Konapala G, Mishra A (2017) Review of complex networks application in hydroclimatic extremes with an implementation to characterize spatio-temporal drought propagation in continental USA. J Hydrol 555:600–620. https://doi.org/10.1016/j.jhydrol.2017.10.033. https://www.sciencedirect.com/science/article/pii/S0022169417307096

Kunkel KE, Easterling DR, Kristovich DAR, Gleason B, Stoecker L, Smith R (2012) Meteorological causes of the secular variations in observed extreme precipitation events for the conterminous United States. J Hydrometeorol 13(3):1131–1141. https://doi.org/10.1175/JHM-D-11-0108.1

Lukens KE, Berbery EH, Hodges KI (2018) The imprint of strong-storm tracks on winter weather in North America. J Clim 31(5):2057–2074. https://doi.org/10.1175/JCLI-D-17-0420.1. https://journals.ametsoc.org/view/journals/clim/31/5/jcli-d-17-0420.1.xml

Malik N, Bookhagen B, Marwan N, Kurths J (2011) Analysis of spatial and temporal extreme monsoonal rainfall over south asia using complex networks. Clim Dyn 39:1–17. https://doi.org/10.1007/s00382-011-1156-4

Merz B, Blöschl G, Vorogushyn S, Dottori F, Aerts J, Bates P, Bertola M, Kemter M, Kreibich H, Lall U, Macdonald E (2021) Causes, impacts and patterns of disastrous river floods. Nature Reviews Earth & Environment 2:1–18. https://doi.org/10.1038/s43017-021-00195-3

Molkenthin N, Rehfeld K, Marwan N, Kurths J (2014) Networks from flows - from dynamics to topology. Sci Rep 4(4119):1–5. https://doi.org/10.1038/srep04119. http://www.nature.com/srep/2014/140218/srep04119/full/srep04119.html

Mondal S, Mishra AK (2021) Complex networks reveal heatwave patterns and propagations over the USA. Geophys Res Lett 48(2):e2020GL090411. https://doi.org/10.1029/2020GL090411. https://agupubs.onlinelibrary.wiley.com/doi/abs/10.1029/2020GL090411

Mondal S, Mishra AK, Leung LR (2020) Spatiotemporal characteristics and propagation of summer extreme precipitation events over United States: a complex network analysis. Geophys Res Lett 47(15):e2020GL088185. https://doi.org/10.1029/2020GL088185

Mullen SL (2008) Spatiotemporal variability of hourly precipitation over the eastern contiguous United States from stage IV multisensor analyses. J Hydrometeorol 9(1):3–21. https://doi.org/10.1175/2007JHM856.1. https://journals.ametsoc.org/view/journals/hydr/9/1/2007jhm856_1.xml

Najibi N, Mazor A, Devineni N, Mossel C, Booth JF (2020) Understanding the spatial organization of simultaneous heavy precipitation events over the conterminous United States. Journal of Geophysical Research: Atmospheres 125(23):e2020JD033036. https://doi.org/10.1029/2020JD033036. https://agupubs.onlinelibrary.wiley.com/doi/abs/10.1029/2020JD033036

Newman MEJ (2010) Networks: an introduction. Oxford University Press, New York. https://doi.org/10.1093/ACPROF:OSO/9780199206650.001.0001

Ozken I, Eroglu D, Breitenbach SFM, Marwan N, Tan L, Tirnakli U, Kurths J (2018) Recurrence plot analysis of irregularly sampled data. Phys Rev E 98:052215. https://doi.org/10.1103/PhysRevE.98.052215

Ozken I, Eroglu D, Stemler T, Marwan N, Bagci GB, Kurths J (2015) Transformation-cost time-series method for analyzing irregularly sampled data. Phys Rev E 91:062911. https://doi.org/10.1103/PhysRevE.91.062911

Ozturk U, Malik N, Cheung K, Marwan N, Kurths J (2019) A network-based comparative study of extreme tropical and frontal storm rainfall over Japan. Clim Dyn 53(1–2):521–532. https://doi.org/10.1007/s00382-018-4597-1

Quian Quiroga R, Kraskov A, Kreuz T, Grassberger P (2002) Performance of different synchronization measures in real data: a case study on electroencephalographic signals. Phys Rev E 65:041903. https://doi.org/10.1103/PhysRevE.65.041903

Radebach A, Donner RV, Runge J, Donges JF, Kurths J (2013) Disentangling different types of El Niño episodes by evolving climate network analysis. Phys Rev E 88(5):052807

Ralph FM, Rutz JJ, Cordeira JM, Dettinger M, Anderson M, Reynolds D, Schick LJ, Smallcomb C (2019) A scale to characterize the strength and impacts of atmospheric rivers. Bull Am Meteor Soc

100(2):269–289. https://doi.org/10.1175/BAMS-D-18-0023.1. https://journals.ametsoc.org/view/journals/bams/100/2/bams-d-18-0023.1.xml

Rheinwalt A, Marwan N, Kurths J, Werner P, Gerstengarbe FW (2012) Boundary effects in network measures of spatially embedded networks. EPL (Europhysics Letters) 100(2):28002. https://doi.org/10.1209/0295-5075/100/28002

Sivakumar B, Woldemeskel FM (2014) Complex networks for streamflow dynamics. Hydrol Earth Syst Sci 18(11):4565–4578. https://doi.org/10.5194/hess-18-4565-2014. https://hess.copernicus.org/articles/18/4565/2014/

Stolbova V, Martin P, Bookhagen B, Marwan N, Kurths J (2014) Topology and seasonal evolution of the network of extreme precipitation over the Indian subcontinent and Sri Lanka. Nonlinear Process Geophys 21(4):901–917. https://doi.org/10.5194/npg-21-901-2014. https://npg.copernicus.org/articles/21/901/2014/

Suzuki S, Hirata Y, Aihara K (2010) Definition of distance for marked point process data and its application to recurrence plot-based analysis of exchange tick data of foreign currencies. International Journal of Bifurcation and Chaos 20(11):3699–3708. https://doi.org/10.1142/S0218127410027970

Tabari H (2020) Climate change impact on flood and extreme precipitation increases with water availability. Scientific Reports 10

Touma D, Michalak AM, Swain DL, Diffenbaugh NS (2018) Characterizing the spatial scales of extreme daily precipitation in the United States. J Clim 31(19):8023–8037. https://doi.org/10.1175/JCLI-D-18-0019.1

Tsonis A, Roebber P (2004) The architecture of the climate network. Physica A 333:497–504. https://doi.org/10.1016/j.physa.2003.10.045. https://www.sciencedirect.com/science/article/pii/S0378437103009646

Tsonis AA, Swanson KL, Wang G (2008) On the role of atmospheric teleconnections in climate. J Clim 21(12):2990–3001. https://doi.org/10.1175/2007JCLI1907.1. https://journals.ametsoc.org/view/journals/clim/21/12/2007jcli1907.1.xml

Tupikina L, Molkenthin N, López C, Hernández-García E, Marwan N, Kurths J (2016) Correlation networks from flows. The case of forced and time-dependent advection-diffusion dynamics. PLoS ONE 11(4):e0153703. https://doi.org/10.1371/journal.pone.0153703

Victor JD, Purpura KP (1997) Metric-space analysis of spike trains: theory, algorithms and application. Netw Comput Neural Syst 8(2):127–164

Vu TM, Mishra AK (2019) Nonstationary frequency analysis of the recent extreme precipitation events in the United States. J Hydrol 575:999–1010. https://doi.org/10.1016/j.jhydrol.2019.05.090

Weather BD (2021) For Environmental Information (NCEI) CDNC: summary stats — billion-dollar weather and climate disasters — national centers for environmental information (ncei). https://www.ncdc.noaa.gov/billions/summary-stats/US/2010-2020. Accessed 11 October 2021

Wiedermann M, Donges JF, Kurths J, Donner RV (2017) Mapping and discrimination of networks in the complexity-entropy plane. Phys Rev E 96:042304. https://doi.org/10.1103/PhysRevE.96.042304

Wolf F, Bauer J, Boers N, Donner RV (2020) Event synchrony measures for functional climate network analysis: a case study on South American rainfall dynamics. Chaos: An Interdisciplinary Journal of Nonlinear Science 30(3):033102. https://doi.org/10.1063/1.5134012

Woodruff J, Irish J, Camargo S (2013) Coastal flooding by tropical cyclones and sea-level rise. Nature 504:44–52. https://doi.org/10.1038/nature12855

Xiong Y, Ren X (2021) Influences of atmospheric rivers on north pacific winter precipitation: climatology and dependence on ENSO condition. J Clim 34(1):277–292. https://doi.org/10.1175/JCLI-D-20-0301.1. https://journals.ametsoc.org/view/journals/clim/34/1/jcliD200301.xml

Zhang Y, Wang K (2021) Global precipitation system size. Environ Res Lett 16(5):054005. https://doi.org/10.1088/1748-9326/abf394